On the Self-Assembly of a Highly Selective Benzothiazole-Based TIM Inhibitor in Aqueous Solution

ARTICLE *in* LANGMUIR · OCTOBER 2010

Impact Factor: 4.46 · DOI: 10.1021/la102916x · Source: PubMed

6 AUTHORS, INCLUDING:

M. Pilar Gárate
Universidad Técnica Federico Santa María
10 PUBLICATIONS **38** CITATIONS
SEE PROFILE

Luis Espinoza
Universidad Técnica Federico Santa María
61 PUBLICATIONS **208** CITATIONS
SEE PROFILE

Ángel Piñeiro
University of Santiago de Compostela
54 PUBLICATIONS **1,041** CITATIONS
SEE PROFILE

Juan M. Ruso
University of Santiago de Compostela
163 PUBLICATIONS **2,043** CITATIONS
SEE PROFILE

Langmuir
Article
pubs.acs.org/Langmuir

On the Self-Assembly of a Highly Selective Benzothiazole-Based TIM Inhibitor in Aqueous Solution

Natalia Hassan,[†] M. Pilar Gárate,[‡] Tania Sandoval,[‡] Luis Espinoza,[‡] Ángel Piñeiro,*[,†] and Juan M. Ruso*[,†]

[†]*Soft Matter and Molecular Biophysics Group, Department of Applied Physics, University of Santiago de Compostela, Campus Vida s/n, 15782, Santiago de Compostela, Spain, and* [‡]*Departamento de Ingeniería Química y Ambiental, Universidad Técnica Federico Santa María, Av. Vicuña Mackenna 3939, Santiago, Chile*

Received April 26, 2010. Revised Manuscript Received September 17, 2010

Benzothiazole is a common scaffold on which many bioactive structures, including protein inhibitors and biosensors, are based. The potential self-aggregation of such molecules to form nanoparticles is relevant for a number of practical applications. 3-(2-Benzothiazolylthio)-propanesulfonic acid (BTS) has been reported as a powerful and selective inhibitor of triosephosphate isomerase from *Trypanosoma cruzi*, the parasite that causes the Chagas' disease. Electrical conductivity, sound velocity, density, and nuclear magnetic resonance experiments as a function of temperature and of NaCl concentration have been performed in the present work to provide a comprehensive physicochemical description of this compound in aqueous solution. Molecular dynamics simulations of the same system were also performed to characterize the structure and dynamic behavior of the corresponding aggregates at several concentrations of BTS.

1. Introduction

Natural and artificially designed amphiphilic molecules are widely employed in multiple industries−diagnosis tools, drug development, cosmetics, paints, or food processing−as well as in consumer products. For this reason their study changed from being originally considered as a branch of fundamental science to be essential in nano and biotechnology applied research. For applications in drug delivery, previous reports revealed that nanoparticles with different sizes and structures would bind to different tissues and organs. Their thermal and mechanical stabilities are interesting issues that should be considered to increase their blood circulation time, thus contributing to reduce side effects. Molecular architecture is a key factor in the design of self-assembling systems for nanoparticle preparation.[1] Structural information of the aggregates, like the packing parameter, directly related with the amphiphile molecule structure and with its hydrophilic/hydrophobic balance, as well as thermodynamic properties as a function of temperature and of the concentration of the molecule itself or of any cosolute, represent the keystone of the proper analysis that should be done on new molecules with biomedical applications.[2−4]

A number of pharmaceutical targets are susceptible to being inhibited by amphiphilic molecules with one or more aromatic nuclei.[5] Previous studies have focused on the self-assembly properties of the benzothiazole ring.[6] Benzothiazole derivatives have been widely employed in both therapeutic treatments and diagnosis including amyloid-β markers and dyes to sense protein conformational changes in living cells.[7] It has been demonstrated that a series of benzothiazoles substitutes are selective and high affinity inhibitors of different triosephosphate isomerases (TIM) including *Tripanosome cruzi* (Tc) and *Tripanosome brucei* (Tb) TIMs. These tripanosomes are flagellated protozoa responsible for American and African tripanosomiasis, parasitic sicknesses currently considered as emerging infectious diseases[8] that eventually end in patient death. In spite of their prevalence in endemic regions and of their increasing propagation over the whole world,[9] effective treatments for trypanosomiasis are still a challenge. 3-(2-Benzothiazolylthio)-propanesulfonic acid (BTS; see Figure 1) is one of the recently developed species-selective TIM inhibitors proposed to treat tripanosomiasis.[10,11] Although the structure of the complex formed by only one BTS molecule and TcTIM was crystallized, with the ligand located at the interface between the two enzyme subunits, kinetic and thermodynamic studies showed that at least two BTS molecules per enzyme are needed for inactivation.[12] On the other hand, it has been shown that premature aggregation of amphiphilic molecules below the

*Corresponding authors. E-mail: Angel.Pineiro@usc.es; JuanM.Ruso@usc.es. Tel.: +34 981 563 100. Fax: +34 981 520 676.

(1) (a) Cheng, L.; Cao, D. *Langmuir* **2009**, *25*, 2749–2756. (b) Ariga, K.; Hill, J. P.; Lee, M. V.; Vinu, A.; Charvet, R.; Acharya, S. *Sci.Technol. Adv. Mater.* **2008**, *9*, 14109–14109. (c) Klok, H. A.; Lecommandoux, S. *Adv. Mater.* **2001**, *13*, 1217–1229. (d) Davis, J. T.; Spada, G. P. *Chem. Soc. Rev.* **2007**, *36*, 296–313.

(2) Israelachvili, J. N.; Mitchell, D. J.; Ninham, B. W. *J. Chem. Soc., Faraday Trans. 2* **1976**, *72*, 1525–1567.

(3) Farias, T.; de Menorval, L. C.; Zajac, J.; Rivera, A. *Colloid Surf. A* **2009**, *345*, 51–57.

(4) Kopecka, B.; Fazekas, T.; Kaclik, P.; Kopecky, F. *Tenside, Surfactants, Deterg.* **2009**, *46*, 169–174.

(5) Schreier, S.; Malheiros, S. V. P.; Paula, E. *Biochim. Biophys. Acta* **2000**, *1508*, 210–234.

(6) (a) Roulia, M.; Vassiliadis, A. A. *Microporous Mesoporous Mater.* **2009**, *122*, 13–19. (b) Kuroda, S. *Adv. Colloid Interface Sci.* **2004**, *111*, 181–209. (c) Sovenyhazy, K. M.; Bordelon, J. A.; Petty, J. T. *Nucleic Acids Res.* **2003**, *31*, 2561–2569.

(7) (a) Henriksen, G.; Hauser, A. I.; Westwell, A. D.; Yousefi, B. H.; Schwaiger, M.; Drzezga, A.; Wester, H.-J. *J. Med. Chem.* **2007**, *50*, 1087–1089. (b) Mathis, C A.; Wang, Y.; Holt, D. P.; Huang, G.-F.; Debnath, M. L.; Klunk, W. E. *J. Med. Chem.* **2003**, *46*, 237–243. (c) Toutchkine, A.; Kraynov, V.; Hahn, K. *J. Am. Chem. Soc.* **2003**, *125*, 4132–4145.

(8) Jones, K E.; Patel, N. G.; Levy, M. A.; Storeygard, A.; Balk, D.; Gittleman, J. L.; Daszak, P. *Nature* **2008**, *451*, 990–993.

(9) Schmunis, G. A. *ISBT Sci. Ser.* **2007**, *2*, 6–11.

(10) Briceño-Leon, R. *Cad. Saúde Pública, Rio de Janeiro* **2009**, *25*(Sup1), 71–82.

(11) Téllez-Valencia, A.; Ávila-Ríos, S.; Pérez-Montfort, R.; Rodríguez-Romero, A.; Gómez-Puyou, M. T.; López-Calahorra, F.; Gómez-Puyou., A. *Biochem. Biophys. Res. Commun.* **2002**, *295*, 958–963.

(12) Téllez-Valencia, V.; Olivares-Illana, A.; Hernández-Snatoyo, R.; Pérez-Montfort, M.; Costas, A.; Rodríguez-Romero, F.; López-Calahorra, M. T.; Gómez-Puyou, A; Gómez-Puyou, J. *Mol. Biol.* **2004**, *341*, 1355–1356.

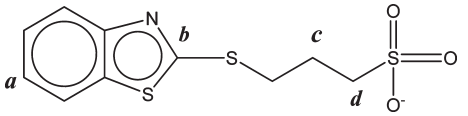

Figure 1. BTS molecule two-dimensional structure. The a−d labels correspond to the groups considered in the NMR analysis.

corresponding critical aggregation concentration induced by the presence of macromolecules is possible.[13] These findings, together with our own interest in drug self-assembly,[14] drug−protein interaction,[15,16] and even TcTIM (the actual target of BTS),[17] encouraged us to perform the present comprehensive study of BTS self-assembly as a function of its concentration, temperature, and also salt concentration. The potential effect of pH changes was not considered in the present work since it is not expected to be serious due to the relatively low pK_a value of BTS (~1.2) when compared to the pH of most representative biological environments (~3 in the stomach, ~5 in the small intestine and ~7.4 in blood). The results are expected to provide useful information for potential pharmaceutical developments based on BTS and, in general, with benzothiazole as a common scaffold.

2. Methods

2.1. Materials. BTS (> 97% purity) was purchased from Aldrich Lancaster. All measurements except NMR were performed using distilled water with conductivity below 3 μS cm^{-1} as a solvent. The solutions were prepared at 298.15 K as indicated in the following section. For nuclear magnetic resonance experiments, deuterated water (> 99.99% purity) purchased from Sigma-Aldrich G.A was used as the solvent. The pH of BTS solutions was 5.5.

2.2. Experimental Methods. Conductivities were measured using a Kyoto Electronics conductometer model CM-117 with a K-121 cell type. The cell constant was determined using KCl solutions following the procedure suggested by Monk.[18] All measurements were performed in a PolyScience model PS9105 thermostatted water bath, at the required constant temperature within ±0.05 K. Conductivity isotherms were obtained by continuous dilution of a concentrated sample, prepared by weight. The expected duration of the dynamics processes varies from 10^{-8} to 10^{-2} s, i.e., between typical aggregate−solvent exchange time of amphiphilic molecules and typical fusion time of the corresponding aggregates. Thus, the equilibrium is guaranteed a few seconds after dilution.[19]

Ultrasound velocities and densities were continuous, simultaneous and automatically measured using a DSA 5000 Anton Paar density and sound velocity analyzer. This equipment possesses a new generation vibrating tube for density measurements and a stainless-steel cell connected to a sound velocity analyzer with resolution ±10^{-6} g cm^{-3} and 10^{-2} m s^{-1}, respectively. Both speed of sounds and densities are extremely sensitive to temperature, so this was controlled to within ±10^{-3} K through a Peltier device incorporated in the equipment. Each sample was measured three times, and standard deviations were found to be 10^{-6} g cm^{-3} and 10^{-2} m s^{-1}, respectively. The temperature range was from 288.15 to 318.15 K and the NaCl concentrations from 0.00 to 0.20 mol kg^{-1}.

The samples for NMR experiments were prepared directly in the spectrometer tubes, by adding solvent and BTS using micropipets to achieve the desired concentration. Three concentrations (50, 160 and 270 × 10^{-3} mol kg^{-1}) of BTS pure water solutions as well as in the presence of 0.05, 0.10, and 0.20 mol kg^{-1} of NaCl were employed for these experiments. The spectra were recorded at 400.132 MHz, 300 K and 1 bar, using a Bruker AVANCE 400 Digital NMR spectrometer containing an inverse detection probe of type BBI 5 mm 1H-BB, with gradient units Z-GRD Z8202/0253. Diffusion-ordered spectroscopy (DOSY) experiments, based on pulse-field gradient spin−echo ^{1}H NMR, were performed to determine the diffusion coefficient of each species in the sample. The signal of residual water in the solvent was taken as the reference. The diffusion coefficients are calculated by using the Stejskal−Tanner equation

$$A = A_0 \exp\left[- Dg^2\gamma^2\delta^2\left(\Delta - \frac{\delta}{3}\right)\right]$$

where A is the intensity of the signal, A_0 is the intensity of the initial (highest) signal, D is the self-diffusion coefficient, g is the gradient force, γ is the gyromagnetic ratio, δ is the time step of the gradient, and Δ is the diffusion time. All experiments were carried out using a LED sequence (ledbpgp2s pulprog) obtained and optimized from the library of standard parameters from Bruker. For our samples, A_0 was set to 36106812.514, using the residual water signal 4.67 ppm as a reference. γ was set to 2.675197 × 10^4 G^{-1} s^{-1} for ^{1}H, g ranged from 2% to 98%, δ was set to 2 ms, and Δ was set to 200 ms. Using these parameters, the spectrometer generated a DOSY spectrum in which the signals can be seen with ppm on the horizontal axis and the value of log D on the vertical axis.

2.3. Molecular Dynamics Simulations. Three random mixtures consisting of ~6500 waters and 20, 40, or 60 BTS molecules with their corresponding counterions (Na^+ cations) were introduced in cubic boxes of edge length 6 nm. Then, an energy minimization of the system using the steepest descent method was carried out. Trajectories of 50 ns at 298 K and 1 bar were performed for each of the three systems using the GROMACS package[20] version 4.0.5. The GROMOS96 (53a6) force field[21] with partial charges, bond lengths, angles, and proper and improper dihedral parameters obtained by using both the engine and the building blocks repository available at the Automated Topology Builder (ATB) server [http://compbio.chemistry.uq.edu.au/atb/], was employed to model BTS. The simple point charge (SPC) model[22] was utilized for water molecules. Three dimensional periodic boundary conditions were used for all of the trajectories. Water + ions on the one hand and BTS molecules on the other hand were separately coupled to a Nose−Hoover thermostat with a common period of 0.1 ps.[23] The pressure was isotropically controlled by using a Parrinello−Rahman barostat[24] with a coupling constant of 0.5 ps and considering a isothermal compressibility of 4.5 × 10^{-5} bar^{-1}. Long range electrostatic interactions were calculated using the particle mesh Ewald method[25]

(13) Jiang, Y. B.; Wang, X. J. Direct Evidence for β-Cyclodextrin-Induced Aggregation of Ionic Surfactant Below Critical Micelle Concentration. *Appl. Spectrosc.* **1994**, *48*, 1428–1431.
(14) Ruso, J. M.; Attwood, D.; Taboada, P.; Suárez, M. J.; Sarmiento, F.; Mosquera, V. *J. Chem. Eng. Data* **1999**, *44*, 941–943.
(15) (a) Taboada, P.; Attwood, D.; Ruso, J. M.; García, M.; Mosquera, V. *Phys. Chem. Chem. Phys.* **2000**, *2*, 5175–5179. (b) Ruso, J. M.; Taboada, P.; Martinez-Landeira, P.; Prieto, G.; Sarmiento, F. *J. Phys. Chem. B* **2001**, *105*, 2644–2648.
(16) Ruso, J. M.; Deo, N.; Somasundaran, P. *Langmuir* **2004**, *20*, 8988–8991.
(17) Díaz-Vergara, N.; Piñeiro, Á. *J. Phys. Chem. B* **2008**, *112*(11), 3529–3539.
(18) Monk, B. *Electrolytic Dissociation*; Academic Press: London, 1961.
(19) Smit, K.; Essenlink, P. A. J.; Hilbers, N. M.; van Os, L. M. A.; Rupert, I.; Szeleifer *Langmuir* **1993**, *9*, 9–11.
(20) Berendsen, H. J. C.; van der Spoel, D.; van Drunen, R. *Comput. Phys. Commun.* **1995**, *91*, 43–56. (b) Lindahl, E.; Hess, B.; van der Spoel, D. *J. Mol. Model.* **2001**, *7*, 306–317. (c) van der Spoel, D.; Lindahl, E.; Hess, B.; Groenhof, G.; Mark, A. E.; Berendsen, H. J. C. *J. Comput. Chem.* **2005**, *26*, 1701–1718.
(21) Oostenbrink, C.; Villa, A.; Mark, A. E.; van Gunsteren, W. F. *J. Comput. Chem.* **2004**, *25*, 1656–1676.
(22) Berendsen, H. J. C.; Postma, J. P. M.; van Gunsteren, Hermans, J. Interaction models for Water in Relation to Protein Hydration. *Intermolecular Forces*; Pullman, B., Ed.; D. Reidel Publ. Co.: Holland, 1981.
(23) (a) Nosé, S. *Mol. Phys.* **1984**, *52*, 255–268. (b) Hoover, W. G. *Phys. Rew. A* **1985**, *31*, 1965–1975.
(24) (a) Parrinello, M.; Rahman, A. *J. Appl. Phys.* **1981**, *52*, 7182–7190. (b) Nosé, S.; Klein, M. L. *Mol. Phys.* **1983**, *50*, 1055–1076.
(25) (a) Darden, T.; York, D.; Petersen, L. *J. Chem. Phys.* **1993**, *98*, 10089–10092. (b) Essmann, U.; Perera, L.; Berkowitz, M. L.; Darden, T.; Lee, H.; Pedersen, L. G. *J. Chem. Phys.* **1995**, *103*, 8577–8593.

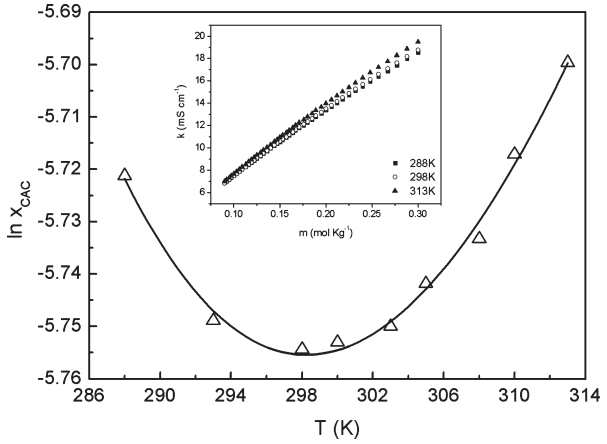

Figure 2. Natural logarithm of the critical aggregation concentration as a function of temperature. The solid line corresponds to the fit of experimental data to eq 1.

with a real-space cutoff of 1.2 nm, a 0.15 nm spaced grid, and fifth-order B-spline interpolation. Random initial velocities were assigned to the systems from a Maxwell−Boltzmann distribution at 298 K. The equations of motion were integrated using the leapfrog method[26] with a time step of 2 fs. Bond lengths and angles in water were constrained using the SETTLE algorithm,[27] and the LINCS algorithm[28] was used to constrain bond lengths within the surfactant molecules. During the MD simulations, coordinates of every particle in the simulation systems were stored every 10 ps for further analysis.

3. Results and Discussion

3.1. Electrical Conductivity Measurements. For the studied temperature range (288−318 K) the electrical conductivity concentration dependence shows a monotonic increase with a slight gradual decrease in slope, as expected for self-assembly processes[29a] (see Figure S1 in the Supporting Information). Critical aggregation concentration (CAC) values were calculated by fitting the experimental isotherms to the nonlinear function obtained by direct integration of a Boltzmann-type sigmoid function.[29b] The CACs obtained by this method as a function of temperature show the typical U-shaped behavior observed for the critical micelle concentration (CMC) of surfactant molecules. For those systems, the CMC decrease with temperature increase, like that observed in Figure 2 at $T <$ 298 K, is typically explained by the net rupture of structured water surrounding the hydrophobic tails, thus promoting micellization.[30a] The opposite trend at higher temperatures (Figure 2) is typically due to the dominant effect coming from the dehydration of the charged head groups accompanied by the subsequent electrostatic repulsion.[30b] Thermodynamic parameters corresponding to the aggregation process can be obtained by analyzing the CAC dependence on temperature. The Rodriguez model[31] was employed to describe this behavior

Table 1. Standard Molar Isobaric Heat Capacities, $\Delta C^0_{P,m}$ (J mol^{-1} K^{-1}), Enthalpies, ΔH^0_m (J mol^{-1}), Entropies ΔS^0_m (J mol^{-1} K^{-1}), and Free Energies of Aggregation, ΔG^0_m (J mol^{-1}), at Different Temperatures (K)

T	$\Delta C^0_{P,m}$	ΔH^0_m	ΔS^0_m	ΔG^0_m
288.15	−495.74	17293	92.3	−9305.3
293.15	−531.89	14178	81.5	−9739.7
298.15	−568.04	11244	71.6	−10122.6
303.15	−604.18	8490	62.5	−10457.7
308.15	−640.33	5918	54.0	−10748.9
313.15	−676.48	3526	46.3	−10999.8
318.15	−712.63	1315	39.3	−11213.9
323.15	−748.78	−715	33.0	−11394.7
328.15	−784.93	−2565	27.3	−11545.5

in the present work

$$\ln x_{CAC} = \ln x^*_{CAC}\left\{1+\beta_1 T^*\left[\frac{1}{2-\beta}\left(\frac{T^*}{T}-2-\frac{\beta_0-2}{\beta_1 T^*}\right)+\frac{1}{2-\beta^*}\left(1+\frac{\beta_0-2}{\beta_1 T^*}\right)\right]\right\}+\frac{\Delta C^{0*}_{P,m}}{(2-\beta)R}\left(1-\frac{T^*}{T}-\ln\frac{T}{T^*}\right)+\frac{\alpha}{(2-\beta)R}\left(\frac{T^{*2}-T^2}{2T}+T^*\ln\frac{T}{T^*}\right) \quad (1)$$

where the degree of ionization dependence on temperature, $\beta = \beta_0 + \beta_1 T$ (0.8 and −0.0005 for β_0 and β_1, respectively) and the standard change in isobaric molar heat capacity, $\Delta C^0_{P,m} = \Delta C^{0*}_{P,m} + \alpha(T - T^*)$, are explicitly considered. ln x^*_{CAC} and T^* correspond to the minimum. Figure 2 shows the fair fit of eq 1 to experimental data. Results obtained from the fitting were 298.2 K, −5.75, −568.37 J mol^{-1} K^{-1}, and 0.87 for T^*, ln x^*_{CAC}, $\Delta C^{0*}_{P,m}$, and α/R respectively. The standard enthalpic and entropic changes due to aggregates formation at the minimum are given by

$$\Delta H^{0*}_m = RT^{*2}\beta_1 \ln x^*_{CAC} \quad (2)$$

$$\Delta S^{0*}_m = \frac{\Delta H^{0*}_m}{T^*}\left(2+\frac{\beta_0-2}{\beta_1 T^*}\right) \quad (3)$$

The dependence of the thermodynamic functions on temperature is obtained from the following expressions:

$$\Delta H^0_m = \Delta H^{0*}_m + \Delta C^{0*}_{P,m}(T-T^*) + (\alpha/2)(T-T^*)^2 \quad (4)$$

$$\Delta S^0_m = \Delta S^{0*}_m + \Delta C^{0*}_{P,m}\ln(T/T^*) + \alpha\{T - T^* - T^*\ln(T/T^*)\} \quad (5)$$

and the standard Gibbs energy of aggregates formation is given by

$$\Delta G^0_m = \Delta H^0_m - T\Delta S^0_m = (2-\beta)RT\ln x_{CAC} \quad (6)$$

where the right side of the equation can be obtained from both the charged phase separation model[32,33] which provides a good approximation for relative comparison if the aggregation number

(26) Hockney, R. W.; Eastwood, J. W. *Computer Simulation Using Particles*, 1st ed.; Adam Hilger: Bristol, 1988.
(27) Miyamoto, S.; Kollman, P. A. *J. Comput. Chem.* **1992**, *13*, 952–962.
(28) Hess, B.; Bekker, H.; Berendsen, H. J. C.; Fraaije, J. G. E. M. *J. Comput. Chem.* **1997**, *18*, 1463–1472.
(29) (a) Moroi, Y. *Micelles: Theoretical and Applied Aspects*; Plenum: New York, 1992.(b) Blanco, E; González-Pérez, A.; Ruso, J. M.; Pedrido, R.; Prieto, G.; Sarmiento, F. *J. Colloid Interface Sci.* **2005**, *288*, 247–260.
(30) (a) González-Pérez, A.; Ruso, J. M.; Romero, M. J.; Blanco, E.; Prieto, G.; Sarmiento, F. *Chem. Phys.* **2005**, *313*, 245–259. (b) Zielinski, R. *J. Colloid Interface Sci.* **2001**, *235*, 201–209.
(31) Rodríguez, J. R.; González-Pérez, A.; Del Castillo, J. L.; Czapkiewicz, J. *J. Colloid Interface Sci.* **2002**, *250*, 438–443.
(32) Mukerjee, P.; Korematsu, K.; Okawauchi, M.; Sugihara, G. *J. Phys. Chem.* **1985**, *89*, 5308–5312.
(33) Shinoda, K.; Hutchinson, E. *J. Phys. Chem.* **1962**, *66*, 577–582.

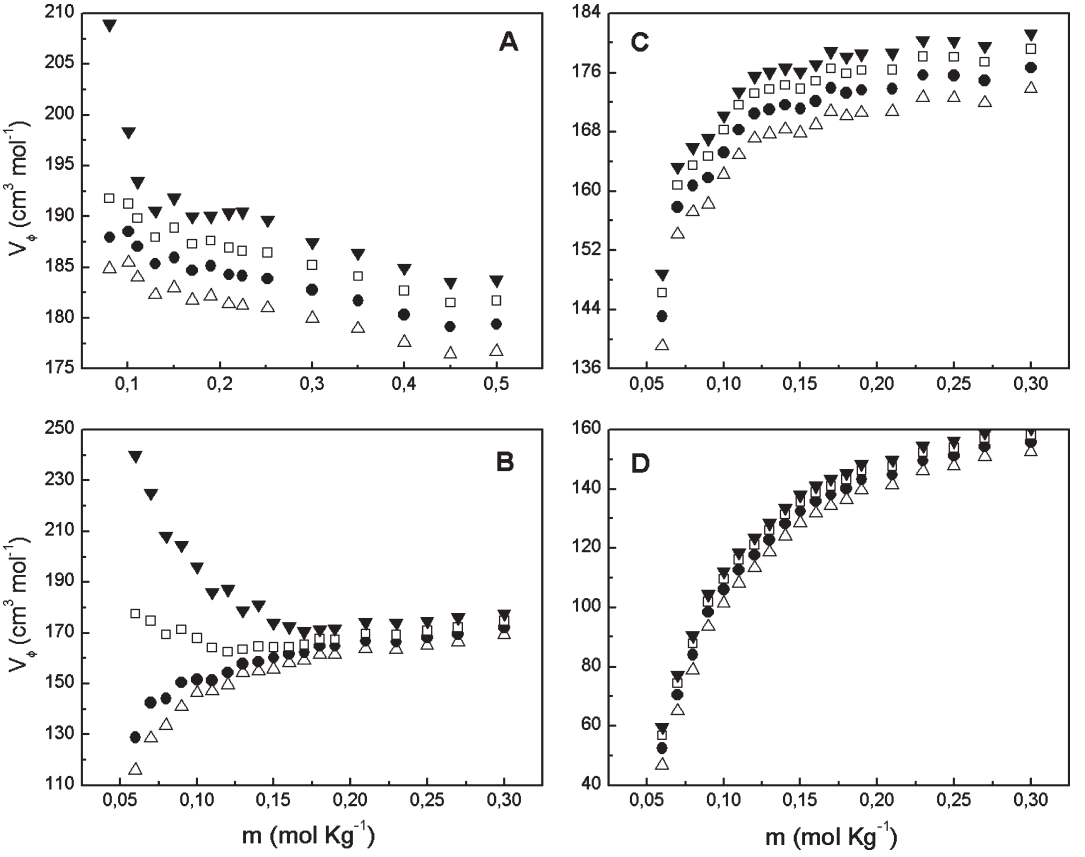

Figure 3. - Apparent molar volumes, V_ϕ, as a function of concentration, m, for different temperatures: (△) 288.15, (●) 298.15, (□) 308.15, and (▼) 318.15 K; and NaCl concentrations: (A) 0.00, (B) 0.05, (C) 0.10, and (D) 0.20 mol kg^{-1}.

is large enough and the mass action model.[34] Heat capacity, enthalpy, entropy, and standard free energy data corresponding to the aggregation process are listed in Table 1. ΔH^0_m and ΔS^0_m are quite sensitive to temperature. ΔH^0_m values indicate that the BTS aggregation is increasingly more exothermic at higher temperatures. Positive values of ΔH^0_m have been attributed to the release of structured water from the hydration layers around the hydrophobic parts of the molecules[35] during the aggregate formation. Such dehydration becomes increasingly negligible with the partial breakdown of the water structure as the temperature increases and the aggregation becomes primarily an enthalpic process. Negative ΔH^0_m values suggest the importance of London-dispersion interactions as the major force for aggregation.[36] However, ΔS^0_m decreased with temperature and remained positive. It has often been found that this kind of aggregation is entropic driven at low temperatures for ionic surfactants whereas enthalpic contributions become more important at high temperatures.[38−40] The above-mentioned higher order of water molecules around hydrocarbon chains at lower temperatures could explain this. Strictly speaking, as the temperature increases the hydrogen bonds between water molecules diminished and therefore less energy was required to break up the water cluster.[37] This fact has been observed not only for many typical surfactants but also for amphiphilic drugs with an aromatic ring like penicillins[39] and betablockers.[40] However, our results show that entropy dominates the aggregation process for the temperature range under study.

3.2. Density and Apparent Molar Volume Measurements. From density measurements, apparent molar volumes can be calculated using the following equation:

$$V_\phi = \frac{10^3(\rho_0 - \rho)}{m\rho\rho_0} + \frac{M}{\rho} \qquad (7)$$

where ρ is the density of the mixture at a given concentration, ρ_0 is the density of pure water, M is the molecular weight of the surfactant, and m is the molality of the solution. Figure 3 shows plots of V_ϕ versus BTS molality at different temperatures and electrolyte concentrations (for clarity, some of the isotherms are shown in the Supporting Information, Figure S2). These plots provide a general overview of the BTS aggregation process. At low concentrations the volumes are strongly dependent on both temperature and electrolyte concentration. This region is characteristic of the monomeric state, showing a significant variation of V_ϕ. The value of the slope in this region presents positive and also negative values depending on the temperature and salt concentration. Negative values are usually considered as a manifestation of the solvophobicity of surfactant molecules and thus account for the solvophobic effect. The solute−solvent interactions cannot be overlooked even in dilute solutions as is done in Debye−Hückel limiting law. Two opposing effects of solvophobicity and charge interactions contribute considerably in determining the sign and

(34) Rusanov, A. I. *Adv. Colloid Interface Sci.* **1993**, *45*, 1–15.
(35) Kresheck, G. C. *Water, A Comprehensive Treatise*; Plenum: New York, 1975.
(36) Nusselder, J. J. H.; Engberts, J. B. F. N. *J. Colloid Interface Sci.* **1992**, *148*, 353–361.
(37) Mehta, S. K.; Bhasin, K. K.; Chauhan, R.; Dham, S. *Colloids Surf. A* **2005**, *255*, 153–157.
(38) Ruso, J. M.; Fontán, J. L.; Prieto, G.; Sarmiento, F. *J. Chem. Phys.* **2003**, *118*, 5964–5970.
(39) Taboada, P.; Attwood, D.; García, M.; Jones, M. N.; Ruso, J. M.; Mosquera, V.; Sarmiento, F. *J. Colloid Interface Sci.* **2000**, *221*, 242–245.
(40) Ruso, J. M.; Attwood, D.; Rey, C.; Taboada, P.; Mosquera, V.; Sarmiento, F. *J. Phys. Chem. B* **1999**, *103*, 7092–7096.

order of the slope. The positive value implies that interactions between the charged species overcome the nonpolar−nonpolar and nonpolar−polar interactions. The change of the slope from negative to positive values indicates strong electrostatic interactions.[41] Similar changes have also been observed for phenothiazine drugs at different pH values.[42] As observed in Figure 3, the apparent molar volumes became constant at high surfactant concentrations. That limits the values that can be taken as the apparent molar volume of a monomer in the aggregate. The concentration dependence of the apparent molar values is generally considered to reflect solute−solute interactions other than the long-range Debye−Hückel type. The apparent molar volumes of this compound change systematically with temperature in the range under study. A vertical translation to higher volumes with temperature is usual. Such behavior was already observed in previous studies for amphiphilic drugs.[43]

Assuming that the additivity rule for the apparent molar volumes and adiabatic compression of the ions in the system stands

$$nV_\phi = n_f V_f + n_c V_c + n_m V_m \quad (8)$$

where V_m is the apparent molar volume of the micelles in the system and n is the total number of BTS moles. n_f, n_c, and n_m are the numbers of moles of free monomers, free counterions, and micelles respectively. Since the studied salt is a 1:1 electrolyte, according the pseudophase separation model below the CAC

$$m_f = m_c = m \quad (9)$$

and above CAC:

$$m_f = \mathrm{CAC} \qquad m_c = \mathrm{CAC} + \beta(m - \mathrm{CAC})$$
$$m_m = (m - \mathrm{CAC})/N_{agg} \quad (10)$$

where N_{agg} is the aggregation number, β is the degree of ionization of micelles, and m_f, m_c, m_m, and m are concentration (molality) of free monomers, free counterions, micelles, and the total concentration, respectively.

Dividing eq 8 by the mass of the solvent (in kg) and taking into account relations 9 and 10 the following set of equations is obtained:

$$V_\phi = (V_f + V_c) \qquad m \le \mathrm{CAC}$$
$$V_\phi = \left(\frac{V_m}{N_{agg}} + \beta V_c\right) - \left(\frac{V_m}{N_{agg}} + (\beta - 1)V_c - V_f\right)\frac{\mathrm{CAC}}{m} \qquad m \ge \mathrm{CAC} \quad (11)$$

Linear fitting of V_ϕ vs $1/m$ in the concentration range above CAC (CAC/$m \le 1$ region) allows us to obtain the value of the apparent molar volume, V_ϕ^{CAC} (intercept + slope), of the surfactant at the CAC, and the change in the apparent molar volume upon aggregation, ΔV_ϕ^{CAC} (slope). The results are collected in Table 2. It is worth to mention that the ΔV_ϕ^{CAC} values of isotherms at different temperatures change from positive, in water, to negative in the presence of salt (Figure S3, Supporting Information). De Lisi et al.[44] attributed the negative slopes observed for ΔV_ϕ^{CAC} of sodium octyl, decyl and dodecyl sulphates in water vs T in the range 298 to 403 K at different pressures to the expansibility of the surfactant in the micellar state being smaller than that in the aqueous phase. Attwood et al.[45] found this decrease with temperature for chlorpromazine an effect which has been attributed to the dehydration of the ionic headgroup. These authors compared their results with those of previous works, finding that negative ΔV_ϕ^{CAC} values are due to micelle formation of lower

Table 2. Apparent Molar Volumes at the CAC, V_ϕ^{CAC} ($cm^3\ mol^{-1}$), Apparent Molar Volume Changes upon Aggregation, ΔV_ϕ^{CAC} ($cm^3\ mol^{-1}$), Isentropic Apparent Molar Adiabatic Compressibilities at the CAC, K_ϕ^{CAC} ($cm^3\ Pa^{-1}\ mol^{-1}$), and Isentropic Apparent Molar Adiabatic Compressibilities upon Aggregation, ΔK_ϕ^{CAC}, of BTS at Different Temperatures (K) and NaCl Concentrations (mol kg^{-1})

T	V_ϕ^{CAC}	ΔV_ϕ^{CAC}	$K_\phi^{CAC}\cdot 10^8$	$\Delta K_\phi^{CAC}\cdot 10^9$
		0.00 NaCl		
283.15	174.05	2.71	0.130	−5.69
288.15	175.55	2.76	0.664	−4.84
293.15	176.90	2.81	1.135	−4.18
298.15	178.14	2.85	1.556	−3.70
303.15	179.30	2.90	1.933	−3.27
308.15	180.39	2.94	2.275	−2.91
313.15	181.42	2.98	2.582	−2.65
318.15	182.32	3.11	2.873	−2.16
323.15	183.56	4.09	3.039	−0.77
		0.05 NaCl		
288.15	173.76	−1.39	0.108	−7.51
298.15	177.64	−1.37	1.243	−6.71
308.15	179.96	−1.32	2.003	−5.78
318.15	182.01	−1.27	2.623	−5.06
		0.10 NaCl		
288.15	170.43	−3.48	0.188	−11.51
298.15	173.00	−3.38	1.312	−10.48
308.15	175.35	−3.32	1.898	−8.78
318.15	180.09	−3.23	2.676	−7.93
		0.20 NaCl		
288.15	153.07	−7.32	−0.480	−19.21
298.15	155.81	−7.12	0.513	−16.92
308.15	158.09	−6.96	1.266	−15.29
318.15	160.51	−6.89	1.915	−14.24

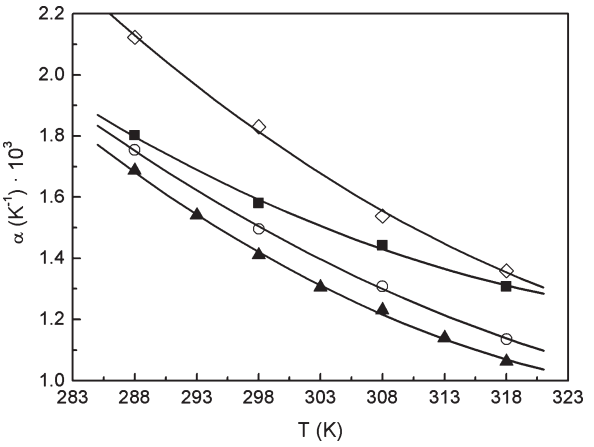

Figure 4. Apparent thermal expansion coefficients, α, as a function of temperature for different NaCl concentrations: (▲) 0.00, (○) 0.05, (■) 0.10, and (◇) 0.20 mol kg^{-1}.

(41) Mehta, S. K.; Sharma, S.; Joshi, I. M. *Colloids Surf. A* **2002**, *196*, 259–267.
(42) Cheema, M. A.; Siddiq, M.; Barbosa, S.; Tabeada, P.; Mosquera, V. *J. Chem. Eng. Data* **2008**, *53*, 368–373.
(43) Ruso, J. M.; González-Pérez, A.; Prieto, G.; Sarmiento, F. *Colloid Surf. B* **2004**, *33*, 165–175.
(44) de Lisi, R.; Milioto, S.; Muretore, N. *Langmuir* **2001**, *17*, 8078–8085.
(45) Attwood, V.; Mosquera, C.; Rey, M.; García *J. Colloid Interface Sci.* **1991**, *147*, 316–320.

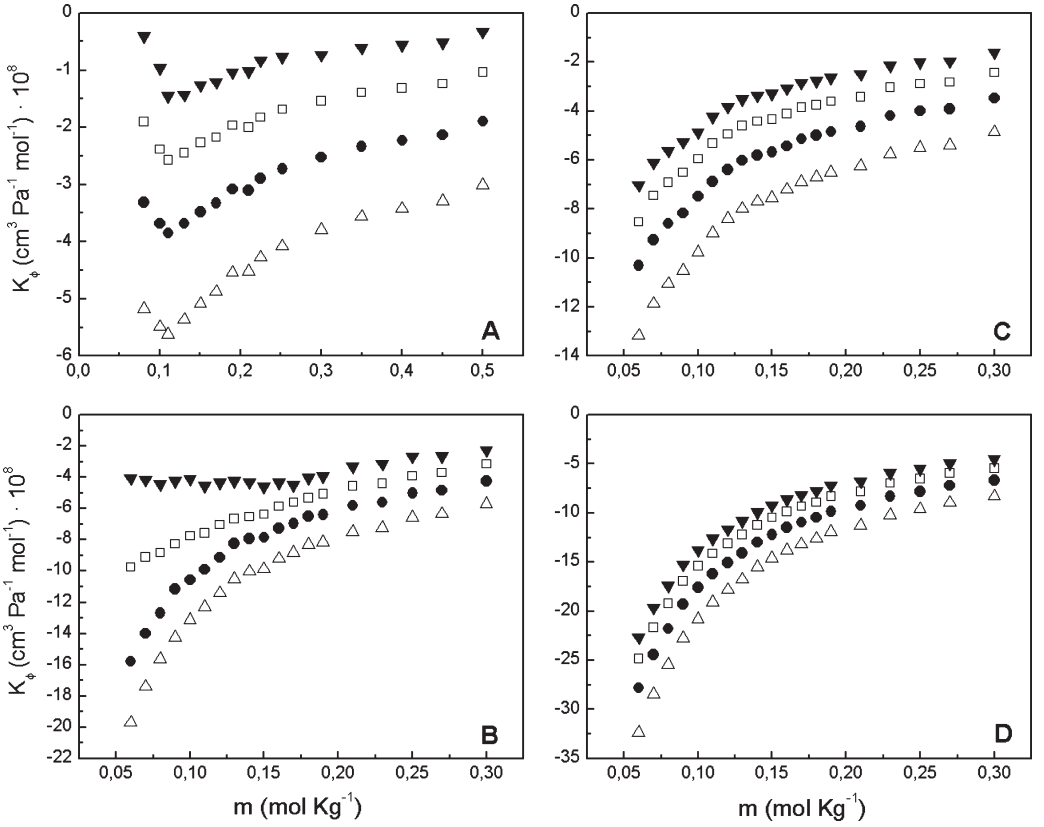

Figure 5. Isentropic apparent molar compressibilities, K_ϕ, as a function of concentration, m, for different temperatures: (△) 288.15, (●) 298.15, (□) 308.15, and (▼) 318.15 K; and NaCl concentrations: (A) 0.00, (B) 0.05, (C) 0.10, and (D) 0.20 mol kg^{-1}.

aggregation numbers. On the other hand, the positive slope observed in the absence of salt could be related to a larger ionization degree and to a better ability to form hydrogen-bonding interactions. Classical surfactants exhibit large positive ΔV_ϕ^{CAC} values due to the release of structured water in the hydration shell of the monomers upon micelle formation, allowing more structural flexibility and, consequently, larger volume available per monomer within the aggregate compared to that in solution.[46] However, ΔV_ϕ^{CAC} values found for BTS are significantly lower than those of classical surfactants. Such small increase in free space of drug molecules during the transition to the micelle state could be a consequence of the BTS stacked arrangement already observed for tricyclic compounds,[47] or simply due to the rigidity of this molecule, undertaking small geometrical changes upon aggregation. It has been reported that apparent thermal expansion coefficients provide information about solute−solute interactions.[48] This property can be calculated from the temperature dependence of the apparent molar volume at constant pressure and number of the solute moles, by using the following expression:

$$\alpha = \left(\frac{1}{V_\phi}\right)\left(\frac{\partial V_\phi}{\partial T}\right)_{p,n_i} \qquad (12)$$

Apparent thermal expansion coefficients (α) of BTS solutions in water and three different concentrations of NaCl (0.05, 0.1, and 0.2 mol kg^{-1}) as a function of T are plotted in Figure 4. The

Table 3. Hydrodynamic Radii (nm) of Aggregates at Different BTS and NaCl Concentrations (mol kg^{-1})

[BTS]	[NaCl]: 0.00	0.05	0.10	0.20
0.050	0.60	0.71	0.77	0.99
0.160	0.90	1.18	1.36	1.81
0.270	1.31	1.67	1.87	2.42

obtained values, with negative slope, are comparable to those found for inorganic salts such as ammonium chloride, ammonium acetate, or ammonium propionate. In general, different α profiles as a function of the concentration indicate a significant dependence on structural features, such as electrical charge, size, type of ion, as well as the relative proportions of the hydrophilic or hydrophobic parts of the molecule.[49] It has been shown that higher α values for the free molecules are related with their stronger hydration compared with that of the monomers in micelles. Accordingly, from the present results the lower values of this parameter at high BTS concentrations (over CAC) indicate a lower hydration of BTS in the aggregated form. The role of salt concentration is also assessed in Figure 4. The higher α values in the presence of salt suggest a higher hydration of BTS molecules when increasing the salt concentration.

3.3. Sound Velocity and Compressibilities. Using the Laplace equation, density and ultrasound velocity measurements were combined to calculate adiabatic compressibilities

$$\beta' = -\frac{1}{V}\left(\frac{\partial V}{\partial P}\right)_S = \frac{10^{-3}}{\rho u^2} \qquad (13)$$

(46) Zielinski, R.; Ikeda, S.; Nomura, H.; Kato, S. *J. Chem. Soc. Faraday Trans. I* **1988**, *84*, 151–163.
(47) Attwood, D.; Waight, R.; Blundell, R.; Bloor, D.; Thevand, A.; Boitard, E.; Dubès, J. P.; Tachoire, H. *Magn. Reson. Chem.* **1994**, *32*, 468–472.
(48) (a) Rudan-Tasic, D.; Klofutar, C. *Monatch. Chem.* **1998**, *129*, 1245–1257. (b) Idqbal, M.; Verrall, R. E. *Can. J. Chem.* **1989**, *67*, 727–734.
(49) Klofutar, C.; Horvat, J.; Rudan-Tasič, D. *Acta Chim. Slov.* **2006**, *53*, 274–283.

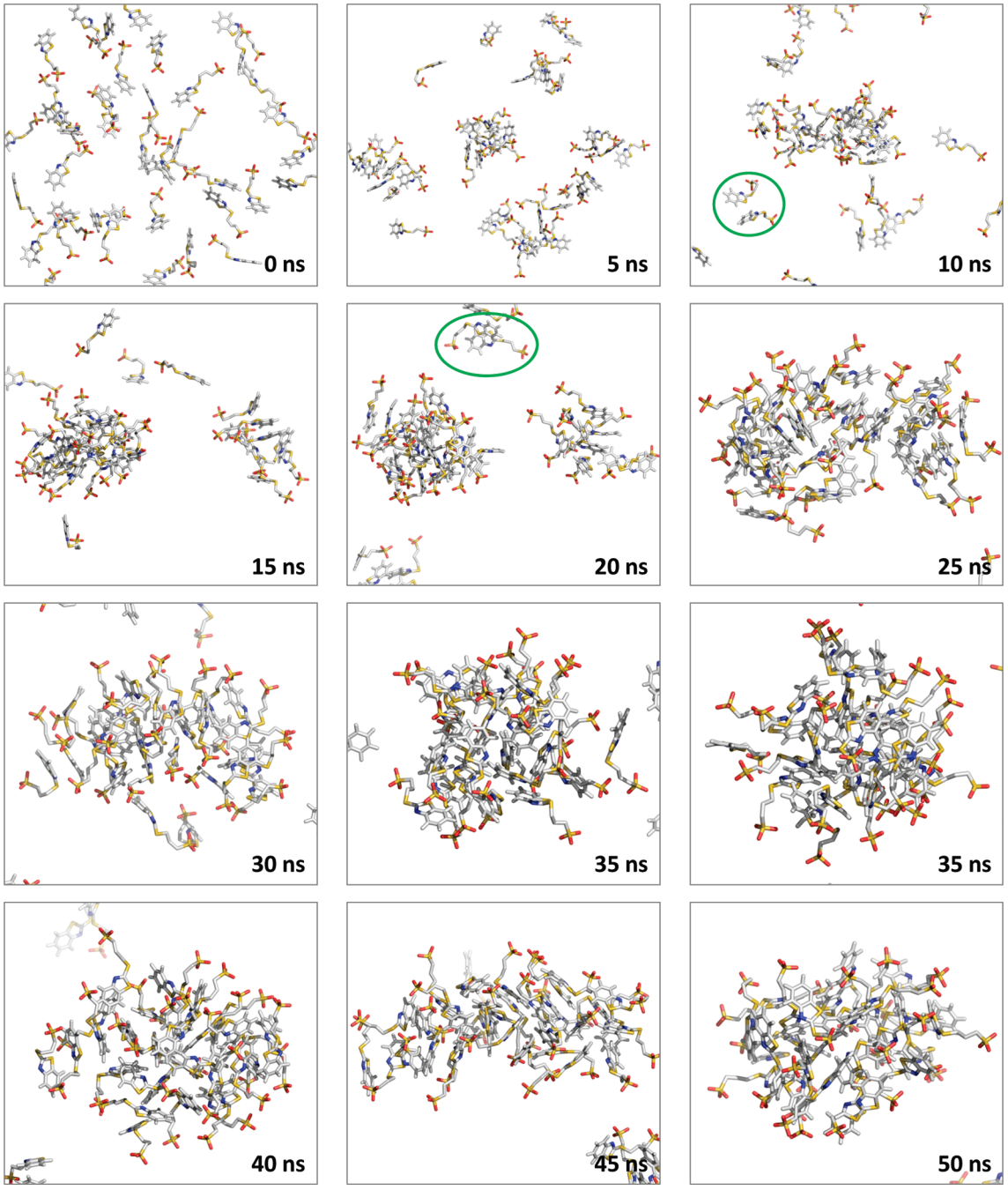

Figure 6. Snapshots taken from a molecular dynamics trajectory for a system with 40 BTS molecules (in sticks representation) and 6513 waters (not shown). The simulation times are indicated in the right lower corner of each image. Two different views are shown for the aggregate at 35 ns. Dimeric structures with the aromatic rings stacked are green-encircled in the snapshots at 10 and 20 ns.

where V, P, and S refer to volume, pressure, and entropy, respectively. β' is the adiabatic compressibility coefficient, expressed in Pa^{-1} when ultrasound velocities u are expressed in cm s^{-1} and densities ρ in g cm^{-3}. Apparent molar isentropic adiabatic compressibilities, K_ϕ, can be calculated from ultrasound measurements

$$K_\phi = \frac{10^3(\beta' - \beta_0')}{m\rho_0} + \beta_0' V_\phi \qquad (14)$$

where β' and β_0' are the isentropic compressibility coefficients of the solution and solvent, respectively. Figure 5 shows plots of K_ϕ vs BTS molality at different temperatures and electrolyte concentrations. Following a procedure similar to that previously explained (eqs 8−11) but substituting V_ϕ, V_m, V_f, and V_c for K_ϕ, K_m, K_f, and K_c, respectively, experimental values for K_ϕ^{CAC} (apparent molar adiabatic compressibility at the CAC) and ΔK_ϕ^{CAC} (apparent molar adiabatic compressibility upon aggregation) can be calculated from linear fittings of K_ϕ vs $1/m$. The values obtained for the systems under study are listed in Table 2. Moreover, since the solute intrinsic compressibility is assumed to be zero, apparent molar compressibility data at infinite dilution provide insight into the compressibility of the hydration layer around the solute molecule. The more negative the solute compressibility the stronger the hydration. Upon aggregation, the hydration of the hydrophobic groups of amphiphilic molecules vanishes and the compressibility of the aggregate by itself becomes the dominant factor. Previous studies of K_ϕ have

shown that this quantity is large and negative for ionic compounds in water, intermediate and positive for mainly hydrophobic solutes, and small and negative for uncharged hydrophilic solutes.[50] When the aggregate is formed, the released water molecules that were in the vicinity of the hydrophobic part of the molecule become bulk water. The water molecules around the hydrophobic part are highly structured, having a rather low compressibility compared to the bulk water. The values calculated for K_ϕ^{CAC} increase linearly with temperature. Meanwhile, those obtained for the absolute values of ΔK_ϕ^{CAC} decrease with T. Previous studies have reported positive ΔK_ϕ^{CAC} values for drugs[51] which were attributed to the predominant role of the decrease in hydrophobic hydration in the association process. The negative values obtained in the present work suggest that the aggregation process of BTS could be related to a different event, probably to steric interactions. In contrast with the temperature dependence, K_ϕ^{CAC} mostly decreases and the absolute values of ΔK_ϕ^{CAC} increases with salt concentration. An earlier study[52] on the influence of NaCl on SDS micelles showed no measurable change in the compressibility-concentration plot gradients above the CMC upon electrolyte addition (0 to 1 mol dm^{-3} NaCl). Although the author of that work concluded that the compressibility of SDS micelles was not affected by the presence of electrolyte, it should be noted that these data, in fact, predict a slight decrease. The same pattern has been found for propanolol and acebutolol.[49] The variation of ΔK_ϕ^{CAC} with electrolyte concentration shown in the present study could be attributed to a decrease in the intramicellar repulsion due to the shielding of the ionic environment or, alternatively, to the increase in the BTS aggregation due to the well-known salting-out effect.[53]

3.4. Nuclear Magnetic Resonance Measurements. BTS self-association has been investigated by high-resolution NMR spectroscopy. The chemical shifts of four selected molecular positions (see Figure 1) were measured from ^{1}H NMR spectra of BTS solutions at concentrations well below and above the CAC. The examination of the magnitude and sign of chemical shift changes upon aggregation, $\Delta\delta$, ($\Delta\delta = \delta_{aggregate} - \delta_{monomer}$), calculated for each position, provides insight into the possible molecular ordering of the aggregates. Upfield shifts indicate that protons are transferred to a less polar environment[54] while downfield shifts indicate stronger interactions with water molecules. The alkyl chain proton chemical shifts in typical spherical aggregates drop in synchrony with a decrease in the packing parameter and in the proton screening on moving outward from the core to the aggregate surface.[55] In the case of BTS, all protons show pronounced upfield shifts upon aggregation, obtaining similar values for all the electrolyte concentration under study: $\Delta\delta$ = 0.23, 0.03, 0.06, and 0.07 for protons a, b, c, and d, respectively (see Table S1 in Supporting Information). The greatest change corresponds to the protons of the aromatic ring system which results from the association to form micelle-like cores. The proton environment of the side-chains was less affected by the association process.

Diffusion ordered 2D NMR (DOSY) spectra of BTS at several concentrations were analyzed. As an example, the ^{1}H NMR and 2D DOSY spectrum of BTS in water (0.0 NaCl) at a concentration of 0.160 mol kg^{-1} are showed in Figure S4 (Supporting Information).

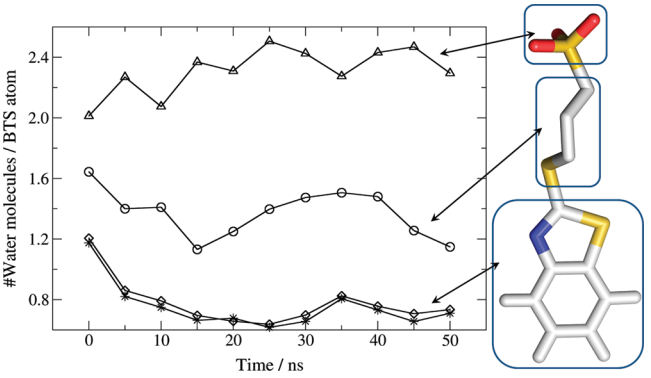

Figure 7. Number of water molecules per atom at less than 4 Å of each of the three groups indicated on the right of the plot, as a function of the simulation time. For the aromatic rings the calculations were performed considering only the heavy atoms (◊) and both the heavy atoms and the hydrogens (*).

It is noteworthy that all signals appear at a single diffusion coefficient with no evidence of polydispersity. Slower core than outer covering diffusion values have been reported. However, DOSY spectra show the whole BTS molecule diffusing in the same way for different concentrations (0.050, 0.160, and 0.270 mol kg^{-1}) both in the absence and in the presence of electrolyte at 0.05, 0.10, and 0.20 NaCl mol kg^{-1}. Using the Stokes−Einstein equation, $D = kT/6\pi\eta R$, where η is the viscosity of D_2O (1.0511 cP at 300 K), which assumes perfectly spherical and noninteracting aggregates hydrodynamic radii were obtained (Table 3).

3.5. Molecular Dynamics Simulations. 50 ns long computational molecular dynamics simulations, following the protocol described in the Methods section, were performed for simulation boxes with 20, 40, and 60 BTS molecules. The snapshots shown in Figure 6 illustrate both the self-aggregation process observed during the first 25 ns, and the typical behavior of the resulting nanoparticles from 25 to 50 ns. The aggregation time scale is larger than that observed for surfactants with aliphatic chains, and the aggregates are less tight than standard micelles. The hydration level per atom for three segments of the BTS molecule, namely the two rings, the ionic head and the linker joining both is shown in Figure 7. It is clear that, during the trajectory, both the propane linker and the aromatic rings tend to lose the contact with water molecules, in contrast with the sulfonic headgroup that tends to increase its hydration. This is in agreement with the NMR and thermodynamic results obtained at 298 K. Moreover, it is clear from the snapshots that the aromatic rings are oriented toward the core of the structure but they do not exhibit the clear stacking pattern previously observed for other structures based on molecules with aromatic rings. This might be due to the charge of the propanesulfonic groups that would be too close to each other in such structures, producing an important electrostatic repulsion. The latter explanation is supported by the structure of several dimers with stacked rings seen throughout the trajectory, where the charged groups appear oriented toward opposite sides with the BTS molecules in both parallel and antiparallel orientation (see the green-encircled dimers in the snapshots at 10 and 20 ns, respectively). The aggregate diameter estimated from the simulations varies between 2.5 and 3.0 nm while the typical aggregation number of the observed nanoparticles ranges from 28 to 32 BTS molecules.

4. Conclusions

The present work provides experimental and theoretical evidence of the BTS self-aggregation. Such an association process

(50) Ruso, J. M.; González-Pérez, A.; Prieto, G.; Sarmiento, F. *Colloid Surf. B* **2004**, *33*, 165–175.
(51) Taboada, P.; Attwood, D.; Ruso, J. M.; García, M.; Mosquera, V. *Langmuir* **2001**, *17*, 173–177.
(52) Shigerehara, K. *Bull. Chem. Soc. Jpn.* **1966**, *39*, 2332–2335.
(53) Long, F. A.; McDevit, W. F. *Chem. Rev.* **1952**, *51*, 119–169.
(54) Bijma, K.; Engberts, J. B. F. N. *Langmuir* **1997**, *13*, 4843–4849.
(55) Yoshino, A.; Yoshida, T.; Okabayashi, H.; Kamaya, H.; Ueda, I. *J. Colloid Interface Sci.* **1998**, *198*, 319–322.

seems to be entropically driven, as indicated by the thermodynamic analysis. The logarithm of the CAC as a function of temperature is U-shaped, in agreement with most amphiphilic drugs. The aggregate formation in absence of salt is related to a likely larger ionization degree and a better ability to form hydrogen bonds. Nevertheless in the presence of salt the higher degree of salt ions binding on the aggregate surface reduces the repulsive interaction between head groups, thus promoting the aggregates growth. In addition, apparent coefficients of expansibility as well as compressibilities indicate that the aggregation process tends to decrease the intramicellar repulsion, in the presence of salt, due to the shield of the ionic interaction. This process could be explained by the presence of steric interactions producing negatives apparent molar adiabatic compressibility values. Based on the similarities of our volumetric results with other drugs molecules, a BTS arrangement with the aromatic rings toward the core of the structure upon aggregation has been proposed. This fact is supported by the analysis of NMR spectra and molecular dynamics simulations. The size of the self-associated nanoparticles was estimated to be about 2.5−3.0 nm with an aggregation number of ∼30 BTS molecules. On the whole, this work provides comprehensive information of BTS solution properties, helping to increase our understanding of its self-assembly process as well as the structure of the resulting aggregates. The present results are expected to be useful as a reference for the study of other benzothiazole-based molecules.

Acknowledgment. Authors thank Dirección Xeral de Promoción Científica e Tecnológica do Sistema Universitario de Galicia for financial support. Á.P. thanks "Xunta de Galicia" for his "Isidro Parga Pondal" research position. We are grateful to the "Centro de Supercomputación de Galicia" (CESGA) for computing time and for their excellent services.

Supporting Information Available: Figures S1−S5 and Table S1. This material is available free of charge via the Internet at http://pubs.acs.org.